Published in final edited form as:
Contrast Media Mol Imaging. 2014 September ; 9(5): 355–362. doi:10.1002/cmmi.1585.

Minimization of self-quenching fluorescence on dyes conjugated to biomolecules with multiple labeling sites via asymmetrically charged NIR fluorophores

Natalia G. Zhegalova, **Shawn He**, **Haiying Zhou**, **David M. Kim**, and **Mikhail Y. Berezin***
Department of Radiology, Washington University School of Medicine in St. Louis, St. Louis, MO 63110

Abstract

Self-aggregation of dyes even at low concentrations pose a considerable challenge in preparing sufficiently bright molecular probes for in vivo imaging, particularly in the conjugation of near infrared cyanine dyes to polypeptides with multiple labeling sites. Such self-aggregation leads to a significant energy transfer between the dyes resulting in severe quenching and low brightness of the targeted probe. To address this problem, we designed a novel type of dye with an asymmetrical distribution of charge. Asymmetrical distribution prevents the chromophores from π-stacking thus minimizing the energy transfer and fluorescence quenching. The conjugation of the dye to polypeptides showed only a small presence of an H-aggregate band in the absorption spectra and, hence, a relatively high quantum efficiency.

INTRODUCTION

The advancement of molecular imaging resulted in the discovery of novel biomarkers and the development of many target-specific molecules from monoclonal antibodies to monobodies, small bodies, polypeptides, proteins, RNA, nanoparticles and small molecules. Conjugation of near-infrared (NIR) dyes to a variety of the targeting molecules has been established as a powerful method for preclinical imaging of tumors (1,2), inflammatory diseases (3,4) and the peripheral nervous system (5).

However, efficient conjugation of fluorescent dyes to targeting macromolecules with multiple labeling sites remains challenging. For example, a typical IgG antibody molecule has 90 lysine residues, many of which are located close to each other (PDB database of IgG, entry 1HZH(6)). Even at low dye-to-protein ratios, the self-aggregation of the dye becomes substantial due to preferential labeling of the neighboring residues caused by a self-assembly of the dyes at the surface of the substrate (7). This results in a clustering of the dye molecules, significant quenching (up to 90%) of the fluorescence, and low brightness (measured as emission power molar absorptivity) of the imaging probe. To address this issue, Wagonner et al (7) suggested to modify benzoindole groups of polymethine dyes with charged groups, such as sulfonate. Such structural modifications have been shown to

*corresponding author: tel. 314-747-0701, berezinm@mir.wustl.edu.

significantly decrease the dye-to-dye interactions and increase the brightness of the probe. However, this did not eliminate the problem entirely.

Herein, we further optimized the structure of the labeling dye to minimize quenching. Our approach was to eliminate the self-aggregation of the dyes by increasing the asymmetry of the charge density on the chromophore. We hypothesized that the asymmetry would lead to the repulsion of the fluorophores from each other in a twisted fashion similar to the geometry illustrated in Fig. 1. With such architecture of increased torsional angles, we expected to decrease the quenching of the dyes by breaking both strong and weak couplings between the individual dyes on the surface of the protein.

RESULTS

We prepared an asymmetrically charged fluorophore LS755 (Fig. 2) via the synthesis shown in Scheme 1. The dye was structurally similar to a previously published NIR dye LS601 (8,9) that showed aggregation upon conjugation to macromolecules such as IgG (see below). In LS755 one of the carboxylic groups is replaced with a sulfonate group. In a free non-conjugated form, both indoles from each dye carry charges. Upon conjugation, only one charge at the indole part remains.

Briefly, indole **3** was prepared via Fischer indole synthesis (10) from 4-hydrazinylbenzenesulfonic acid (**1**) and 3-methylbut-2-one (**2**). Known indolium salts **7** (11) and **8** (8) were prepared by alkylation of the corresponding indoles **4** and **6** with 1,3-propanesultone. Pre-activation of the Vilsmeier type reagent **9** with acetic anhydride was followed by addition of the indolium salt **7** (1.5:1 molar ratio) and acetic acid using standard procedures (12–15). After four hours of stirring at reflux temperature, acetic acid was evaporated, the residue was washed with ethyl acetate several times to remove the unreacted reagent **9**. Ethyl acetate was removed under vacuum and the intermediate **10** (hygroscopic) was immediately transferred to a vial, dissolved in acetic anhydride and pyridine (1:1) solvent ratio. Indolium salt **8** was added and the vial was heated to 110 °C for 10 min. The reaction was followed by the appearance and growth of an absorption peak at ca. 750 nm corresponding to the desired LS755 product and the vanishing of the 506 nm peak of the acetate form of the half-dye. Upon completion, the mixture was cooled, triturated with ethyl acetate, filtered, washed with ethyl acetate and 2-propanol, and dried under reduced pressure and purified on a reverse phase column. The major product in the reaction mixture was found to be LS755 (>80 area % in LCMS).

The conjugation of the dye to the amines on proteins occurred efficiently with high yield via conventional NHS chemistry as we described previously (8). For that, the carboxylic group of LS755 was converted into a corresponding NHS-ester in the presence of EDC (Scheme 1). The pre-activated dye LS755-NHS in the lyophilized form was stable for at least several months. The coupling reactions to polypeptides were conducted in a bicarbonate buffer, and the products were purified by Sephadex columns. The conjugation of LS755 to the macromolecules and purity of conjugates were accessed by SDS-PAGE (Fig. 3). Single-chained proteins BSA and lysozyme showed bands corresponding to their molecular weights, and IgG composed of four peptide chains showed bands corresponding to their

heavy and light chains. A conjugate LS755-PEG_{40kD} was used as a molecular weight marker and showed a single spot on the gel. A free dye LS755-NHS appeared at the bottom of the gel near 1 kDa as expected. The purified conjugates showed no free dye.

Upon conjugation, the dyes were expected to become non-symmetrically charged under physiological conditions given the pKa's of carboxylic acid and sulfonate are in the range of pKa 3–4. Molecular modeling with MM3/PM5 parameters demonstrated that the charges are localized on the indole parts without delocalization across the conjugate system of the dyes (Fig. 4). Expectedly, the charge imposed by sulfonate-carrying indole (in LS755) was significantly higher than that in LS601 leading to a strong charge asymmetry of the dye in a dye conjugate system.

The replacement of a carboxylic group in LS601 with sulfonate (LS755) caused a 7–10 nm hypsochromic shift in absorption and emission spectra. Sulfonate is more electronegative and therefore, is expected to cause a bathochromic shift opposite to what was expected. However, the results are in agreement with Kuhn's rationale for unsymmetrical dyes that predicts a blue shift in unsymmetrical polyenes (16).

The most dramatic change between the dyes was observed in the shape of the absorption peaks of dye-peptide aggregates. The aggregation of dye molecules, such as cyanines, is commonly recognized as a hypsochromically shifted H-band in the absorption spectra of the conjugates (7,17–22) such as shown in Fig. 5 for an LS601-IgG conjugate. It is generally accepted that H-aggregates are composed of dye molecules stacked in a plane-to-plane fashion. This type of aggregation leads to the undesirable loss of fluorescence (see Discussion). In contrast, the absorption spectra LS755-IgG demonstrated the disappearance of the H-band. Similar disappearance was also observed for other LS755 conjugates (Fig. 6).

The fluorescence lifetime reflects the quenching of the probes, with shorter lifetimes indicating a higher degree of quenching. In solvents with strong solvation powers (DMSO) the fluorescence lifetime of LS755 (1.21 ns) is shorter than that of LS601 (1.29 ns). However, in solvents with weak solvation powers (water), that usually promote aggregation of the cyanine dyes, the lifetime of LS755 was slightly greater (0.43 vs. 0.42 ns for LS601 under the same conditions) reflecting a lower aggregation of LS755. The lifetime difference between the two dyes became even more apparent when measuring their conjugates to IgG (0.65 and 0.53 ns for LS755-IgG and LS601-IgG correspondingly, Fig. 7 and Table 1). The fluorescence lifetime of cyanines in dye-protein conjugates usually increases due to a decrease in the rate of quenching caused by the solvent and the changes in the molecular environment (such as polarity) around the probe (12). Thus, the fluorescence lifetime of the dye conjugates is expected to be within two limits in DMSO and water.

DISCUSSION

Strong coupling as a mechanism of quenching

Absorption—When two identical molecules interact under strong coupling conditions (i.e. parallel orientation and close proximity to each other) several features in the absorption spectra are clearly observed. These include peak broadening, the appearance of an H-band as

seen in Fig. 5, and a hypsochromic shift (23). The formation of the H-band is the most prominent and generally explained in terms of Davydov splitting (21,24) where the excitation is distributed over both molecules. In such case, the excited state is no longer described by two identical wave functions characteristic of two single molecules. The energy level for such an excited state is split into two energy levels with one above and one below the level of the monomers (Fig. 8). Since only one transition from the ground to higher excited level is allowed, the spectra are blue shifted as seen in LS601-IgG.

Fluorescence—Another characteristic feature of strong coupling is the absence of fluorescence. Following the excitation to a higher excited state (high exciton state), the molecule rapidly and nonradiatively returns to the lower exciton energy level. For the parallel oriented dimer, this fast internal conversion process from the upper level to the non-emitting lower state decreases transition probability for a radiative process (25) thus suppressing fluorescence.

Weak coupling as a mechanism of quenching

Absorption—Weak coupling is described in terms of Forster resonance energy transfer (FRET). FRET can occur between like molecules (homoFRET) given that there exists a small Stokes shift and substantial overlap between emission and absorption. In FRET, the transfer of the excitation energy takes place only after the excited donor has become fully vibrationally relaxed to S1, the lowest excited state vibration state (26). Hence, the subsequent energy transfer does not change the absorption spectra of the dyes in contrast to strong coupling and therefore no H-band is expected to be observed.

Fluorescence—Unlike FRET, the energy transfer in homo-FRET, does not affect the fluorescence and, in generally, does not change the fluorescence lifetime of the molecules, but decreases fluorescence anisotropy (26,27). Recent work, however, has demonstrated that in some cases, aggregation of fluorophores can increase the rate of non-radiative emission contributing to its fluorescence lifetime shortening (28,29). During homo-FRET, part of the energy is transferred to the acceptor. The quantum efficiency and the lifetime of the acceptor remains the same, but the emission and the lifetime of the donor decreases. Hence, both the donor and the acceptor are the same species, and the overall measureable fluorescence and lifetime is expected to be lower, although, to a smaller extent than if only the donor was measured. Indeed, LS601-IgG with higher level of aggregation showed a larger fluorescence lifetime change from a free molecule to the conjugated state compared to LS755-IgG. Fluorescence anisotropy usually decreases in homo-FRET, however, this effect is only well pronounced in fluorescence proteins where upon dimerization, the molecular weight does not change significantly. The anisotropy of LS755 increased from 0.155 to 0.2–0.24 in accordance to a substantial change in the molecular weight from 0.7 kDa (free dye) to 15–150 kDa in the conjugates.

Charge asymmetry prevents both mechanisms of quenching

According to the classic presentation of strong coupling, the splitting energy and the intensity of the spectroscopic transitions to the different exciton energy levels depend on the

orientations of the interacting monomers and the distance between them (24). For non-planar transition dipoles, the exciton splitting energy is given by Eq. 1(24)

$$\Delta E = \Delta E_+ - \Delta E_- = \frac{2\mu_M^2}{r^3}(\cos\alpha - 3\cos^2\theta) \quad (1)$$

Where r is the distance between centers of the dipole moments, α is the angle between the two molecular planes defined by the diagram shown in Fig. 9 *A*, and θ is the angle between the polarizations axes and the line of molecular centers.

The theory predicts that the parallel configuration provides the strongest effect in this type of coupling. Fig. 9 *B* shows the modeling of the splitting energy as a function of distance *r*, and the angle between the planes illustrates this. The ΔE is minimal when the angle is close to 90°, even when two dyes are very close to each other. A deviation from 90° leads to a sharp increase in the energy transfer and, hence, to quenching.

Similarly, weak coupling such as observed in homoFRET is also affected by the orientation of dyes and is proportional to the dipole angular orientation k^2 from the known Forster relationship (Eqs 2) (30).

$$E_t = \frac{k^2}{C^{-1}r^6 + k^2} \quad (2)$$

where *r* is the distance between two fluorophores; k^2- the orientation factor; *C* a constant for the system under investigation made up of universal constants, a spectral overlap integral, the quantum yield, and the refractive index of the medium.

The orientation factor k^2 gives the dependence of the interaction between two electric dipoles on their orientations. It can be defined by Eq. 3 (30,31) :

$$k^2 = (\sin\theta_D \sin\theta_A \cos\varphi - 2\cos\theta_D \cos\theta_A)^2 \quad (3)$$

where φ represents the angle between the planes as defined in Fig. 10, *A*; θ_D – is the angle between the donor dipole and *R;* and the vector from the donor to the acceptor, $\theta_{A\text{-}}$, is the angle between the acceptor dipole and *R*.

The orientation factor spans from 0 for a perpendicular orientation (no energy transfer) to 4.0 for parallel or anti-parallel stacking (maximum energy transfer). Modeling of Eq. 2–3 shown in Fig. 10 *B*, illustrates this relationship. Hence, fluorophores with a non-symmetrical charge distribution, such as in LS755, provide an advantage to minimize stacking and consequently maximizes the brightness of the conjugate.

CONCLUSIONS

In summary, we propose a new type of NIR fluorescent dye with an asymmetrical charge distribution to prevent an aggregation of the dye on the surface of a polypeptide with multiple sites of labeling. The first example of this type, a cyanine dye LS755 was synthesized with a strong negatively charged sulfonate group on one side of the

chromophore. Upon conjugation of LS755 to macromolecules such as antibodies, proteins, and enzymes, a negligible formation of the H-band with high quantum yield and long fluorescence lifetime were observed. This method of labeling opens a pathway to more efficient fluorescent targeting probes with minimum dye aggregation. The latter leads to a lesser amount of the probe and therefore to a safer imaging procedure. Future directions include optimizing the conjugation chemistry to preserve high specificity of biological polypeptides to molecular targets.

EXPERIMENTAL

Materials

High purity water (18.2 MΩ) was used throughout the study. Organic solvents and reagents were obtained from commercial sources (FisherSci, Signal-Aldirich) and used without further purification. N-Hydroxysuccinamide and 1-ethyl-3-(3-dimethylaminopropyl) carbodiimide (EDC) were obtained from Sigma-Aldrich and Pierce correspondingly. Bovine serum albumin (BSA, grade “agarose gel electrophoresis, 99%”), immunoglobulin G (IgG), lysozymes (Lz) were purchased from Sigma-Aldrich. LS601 was prepared as previously published (8), and the conjugates of BSA-LS755, IgG-LS755 and Lysozyme-LS755 were synthesized, purified, and characterized as specified below (see Synthesis).

Optical measurements

UV/Vis spectra of samples were recorded on a Beckman Coulter DU 640 UV-visible spectrophotometer. Steady state fluorescence spectra, fluorescence lifetime and anisotropy were recorded on a Nanolog spectrofluorometer (Horiba Jobin Yvon, Inc.). The photophysical data (steady-state absorption, fluorescence) and lifetime were obtained in DMSO and water. Fluorescence quantum yield (QY) of the samples was measured using relative method with ICG as a standard. Data in the Table 1 show the calculated QY relative to the QY of ICG in DMSO = 0.12 (32). Recent re-measurements of ICG using absolute method provided QY of ICG in DMSO as 0.22 (33,34). Correspondingly, the QY of the samples can be re-calculated accordingly. Fluorescence lifetime of dyes were determined using the time-correlated single photon counting (TCSPC) technique with a 740 nm NanoLed excitation source as described previously (12).

Dye loading

The dye-to-protein (D/P) ratio of the bioconjugates was calculated according to known equations (14,22).

$$D/P = \frac{C_D}{C_P} = \frac{\varepsilon_{P,280} \times A_{D,755}}{\varepsilon_D (A_{280} - k \times A_{D,755})}$$

The molar absorptivity coefficients of the proteins at 280 nm ($\varepsilon_{p,280}$) were set to IgG 190,000 $M^{-1}cm^{-1}$, BSA 44,000 M^{-1} cm^{-1}, lysozyme – 26,000 M^{-1} cm^{-1} according to the manufacturer specifications. The molar absorptivity for dyes were determined to be 161,000 M^{-1} cm^{-1} for LS601 and 134,000 M^{-1} cm^{-1} for LS755. The absorbance of the dye at 280

nm was corrected by the factor $k = A_{D,280}/A_{D,755}$. The degree of labeling per antibody was 1.7 dye/IgG for LS601/IgG and 1.0 dye/IgG for LS755/IgG.

Fluorescence anisotropy

The study was conducted in an L-format with automated Glan-Thompson polarizing prisms controlled by FluorEssence software (Horiba). The anisotropy values for each dye and dye-conjugate were determined at relatively low concentrations with absorption below 0.2 a.u. to avoid aggregation of the dye or agglomeration of the proteins. The details of the procedure were published previously (8).

Synthesis of LS755

Indolium salts **7** and **8** were obtained according to the standard procedures (8,11). In a vial equipped with a stir bar, indolium **7** (267 mg, 0.74 mmol) and N-[5-(phenylamino)-2,4-pentadienylidene]aniline monohydrochloride **9** (Sigma-Aldrich) (315 mg, 1.12 mmol) were added and dissolved in a mixture of Ac_2O (4.4 mL) and AcOH (4.4 mL). The reaction mixture was heated to reflux for 4 hours. The progress of the reaction was monitored by both TLC (R_f =0.93 for **7** and R_f=0.76 for **10**, C18, H_2O-MeOH 1:1) and UV-Vis (disappearance of the absorption peak at 484 nm and the appearance of a strong peak at 502 nm in methanol). Acetic acid was removed with a rotary evaporator and the product was washed with EtOAc three times to remove unreacted **9**. The crude intermediate **10** was dried under vacuum and used in the next step without further purification. The intermediate **10** (6.9 mg, 0.013 mmol) was dissolved in an acetic anhydride (3.35 mL) and pyridine (3.35 mL) mixture. The UV spectrum (in methanol) showed an absorbance maximum at 506 nm for the acetate form of the intermediate. Indolium **8** (0.013 mmol) was added and the reaction mixture was heated at 110 °C for 10 minutes until the mixture turns green with the disappearance of the absorption peak at 506 nm and the appearance of a strong peak at 753 nm. The mixture was cooled to room temperature and triturated with EtOAc to precipitate the dye. The gummy residue was washed with EtOAc and 2-propanol. The product was dried under reduced pressure and purified on a reverse phase C18 column with water-methanol gradient to afford LS755 as green solid, 3.98 mg. Purity >80 area %. ^{1}H NMR (400 MHz, D_2O) δ=8.88 (d, 1H, J=5.6 Hz), 8.77 (d, 1H, J=4.4 Hz), 8.65-8.50 (m, 1H), 8.09-8.04 (m, 1H), 7.81 (m, 1H), 7.71 (m, 1H), 4.30-4.05 (m, 2H), 3.62 (t, 8H, J=6.4 Hz), 3.12-2.99 (m, 3H), 2.98-2.93 (m, 9H), 2.48-2.43 (m, 1H), 2.03-1.96 (m, 9H). ESI-MS *m/z*: 748 [M^+].

Synthesis of LS755 –NHS ester

LS755 (10 mg, 0.014 mmol) was dissolved in DMF and N-hydroxysuccinamide (2.0 eq.) and EDC (4.0 eq.) were added at once. The reaction mixture was stirred overnight at room temperature. Diethyl ether was added to the reaction mixture to precipitate the product. The obtained product was redissolved in a minimal amount of methanol and triturated with diethyl ether. This step was repeated to give the desired NHS-ester as a green solid (>95 area %, 9.49 mg, yield 84%). ^{1}H NMR (400 MHz, CD_3OD) δ 8.02 (s, 1H), 7.95-7.93 (dd, 2H), 7.87-7.82 (t, 2H), 7.68-7.65 (m, 2H), 7.39-7.34 (m, 2H), 6.64-6.61 (d 2H), 4.37- 4.34 (t,

2H), 4.29-4.27 (m, 2H), 3.01-2.95 (m, 4H), 2.27-2.18 (m, 4H), 1.70-1.69 (d, 12H). ESI-MS *m/z*: 846 [M^+].

Conjugation of LS755 to proteins

BSA-LS755 conjugate—BSA (10.8 mg) was dissolved in 400 μL of 0.1 M $NaHCO_3$ buffer and mixed with a solution of LS755-NHS (0.6 mg) in 50 μL DMSO. The reaction mixture was left shaking at room temperature for 3 hours. The conjugate was purified on a Sephadex G-25 column with 1X PBS buffer. Fractions were evaluated using SDS-PAGE gel; those containing the product were collected and lyophilized.

Lysozyme-LS755 conjugate—Lysozyme (Lz) (1.17 mg) from chicken egg white was dissolved in 400 μL of 0.1 M $NaHCO_3$ buffer and mixed with a solution of LS755-NHS (0.6 mg) in 50 μL DMSO. The reaction mixture was left shaking at room temperature for 3 hours. The conjugate was purified on a Sephadex G-25 column with 1X PBS buffer. Fractions were evaluated using SDS-PAGE gel; those containing the product were collected and lyophilized.

IgG-LS755 conjugate—IgG from rat serum (reagent grade >95% by SDS-PAGE) (1 mg) was dissolved in 400 μL of 0.1 M $NaHCO_3$ buffer. LS755-NHS (17 μL) in 1.4 μL DMSO was added to this mixture and was shaken for 3 hours at room temperature. The reaction mixture was purified on a Sephadex G-25 column with 1X PBS buffer. Fractions were evaluated using SDS-PAGE; those containing the product were collected and lyophilized.

SDS-PAGE—An SDS-PAGE was run for each conjugate using a Bio-Rad Any kD Mini-PROTEAN® TGX™ Gel according to the manufacturer protocol (Bio-Rad Laboratories). The gel was imaged using a home-made NIR imaging system equipped deep cooled CCD camera Versarray (Ropper), SWIRON 1.4/23 Compact (Schneider) lens, 720 nm LED based light source (Thorlabs) and 800 nm long pass filter (Thorlabs). The images were acquired with WinView 32 software and processed with ImageJ.

Acknowledgments

We gratefully acknowledge Steven Wang for proofreading the manuscript and suggestions. We also acknowledge the financial support from the National Cancer Institute of the National Institutes of Health (R21CA149814), the National Heart Lung and Blood Institute as a Program of Excellence in Nanotechnology (HHSN268201000046C). We also thank the Washington University Optical Spectroscopy Core facility (NIH 1S10RR031621-01) for spectroscopy measurements.

REFERENCES

1. Koo H, Lee S, Na JH, Kim SH, Hahn SK, Choi K, Kwon IC, Jeong SY, Kim K. Bioorthogonal copper-free click chemistry in vivo for tumor-targeted delivery of nanoparticles. Angew. Chem. Int. Ed. Engl. 2012; 51(47):11836–11840. [PubMed: 23081905]
2. Villaraza AJL, Milenic DE, Brechbiel MW. Improved Speciation Characteristics of PEGylated Indocyanine Green-Labeled Panitumumab: Revisiting the Solution and Spectroscopic Properties of a Near-Infrared Emitting anti-HER1 Antibody for Optical Imaging of Cancer. Bioconjug. Chem. 2010; 21(12):2305–2312. [PubMed: 21073171]

3. Oushiki D, Kojima H, Terai T, Arita M, Hanaoka K, Urano Y, Nagano T. Development and application of a near-infrared fluorescence probe for oxidative stress based on differential reactivity of linked cyanine dyes. J. Am. Chem. Soc. 2010; 132(8):2795–2801. [PubMed: 20136129]
4. Kundu K, Knight SF, Willett N, Lee S, Taylor WR, Murthy N. Hydrocyanines: a class of fluorescent sensors that can image reactive oxygen species in cell culture, tissue, and in vivo. Angew. Chem. Int. Ed. Engl. 2009; 48(2):299–303. [PubMed: 19065548]
5. Gray DC, Kim EM, Cotero VE, Bajaj A, Staudinger VP, Hehir CAT, Yazdanfar S. Dual-mode laparoscopic fluorescence image-guided surgery using a single camera. Biomed. Opt. Express. 2012; 3(8):1880–1890. [PubMed: 22876351]
6. Saphire EO, Parren PWHI, Pantophlet R, Zwick MB, Morris GM, Rudd PM, Dwek RA, Stanfield RL, Burton DR, Wilson IA. Crystal Structure of a Neutralizing Human IgG Against HIV-1: A Template for Vaccine Design. Science. 2001; 293(5532):1155–1159. [PubMed: 11498595]
7. Mujumdar SR, Mujumdar RB, Grant CM, Waggoner AS. Cyanine-Labeling Reagents: Sulfobenzindocyanine Succinimidyl Esters. Bioconjug. Chem. 1996; 7(3):356–362. [PubMed: 8816960]
8. Gustafson TP, Cao Q, Achilefu S, Berezin MY. Defining a polymethine dye for fluorescence anisotropy applications in the near-infrared spectral range. Chemphyschem. 2012; 13(3):716–723. [PubMed: 22302715]
9. Gustafson TP, Yan Y, Newton P, Hunter DA, Achilefu S, Akers WJ, Mackinnon SE, Johnson PJ, Berezin MY. A NIR dye for development of peripheral nerve targeted probes. MedChemComm. 2012; 3(6):685–690. [PubMed: 24575295]
10. Illy H, Funderburk L. Fischer indole synthesis. Direction of cyclization of isopropylmethyl ketone phenylhydrazone. J. Org. Chem. 1968; 33(11):4283–4285.
11. Myochin T, Hanaoka K, Komatsu T, Terai T, Nagano T. Design Strategy for a Near-Infrared Fluorescence Probe for Matrix Metalloproteinase Utilizing Highly Cell Permeable Boron Dipyrromethene. J. Am. Chem. Soc. 2012; 134(33):13730–13737. [PubMed: 22830429]
12. Berezin MY, Lee H, Akers W, Achilefu S. Near infrared dyes as lifetime solvatochromic probes for micropolarity measurements of biological systems. Biophys. J. 2007; 93(8):2892–2899. [PubMed: 17573433]
13. Strekowski L, Mokrosz JL, Wilson WD, Mokrosz MJ, Strekowski A. Stereoelectronic factors in the interaction with DNA of small aromatic molecules substituted with a short cationic chain: importance of the polarity of the aromatic system of the molecule. Biochemistry. 1992; 31(44): 10802–10808. [PubMed: 1384699]
14. Mujumdar RB, Ernst LA, Mujumdar SR, Lewis CJ, Waggoner AS. Cyanine dye labeling reagents: sulfoindocyanine succinimidyl esters. Bioconjug. Chem. 1993; 4(2):105–111. [PubMed: 7873641]
15. Markova LI, Fedyunyayeva IA, Povrozin YA, Semenova OM, Khabuseva SU, Terpetschnig EA, Patsenker LD. Water soluble indodicarbocyanine dyes based on 2,3-dimethyl-3-(4-sulfobutyl)-3H-indole-5-sulfonic acid. Dyes Pigm. 2013; 96(2):535–546.
16. Kuhn H. A quantum mechanical theory of light absorption of organic and similar compounds. J. Chem. Phys. 1949; 17(12):1198–1212.
17. Berlier JE, Rothe A, Buller G, Bradford J, Gray DR, Filanoski BJ, Telford WG, Yue S, Liu J, Cheung C-Y, Chang W, Hirsch JD, Beechem Rosaria P, Haugland JM, Haugland RP. Quantitative Comparison of Long-wavelength Alexa Fluor Dyes to Cy Dyes: Fluorescence of the Dyes and Their Bioconjugates. J. Histochem. Cytochem. 2003; 51(12):1699–1712. [PubMed: 14623938]
18. Pham W, Lai W-F, Weissleder R, Tung C-H. High Efficiency Synthesis of a Bioconjugatable Near-Infrared Fluorochrome. Bioconjug. Chem. 2003; 14(5):1048–1051. [PubMed: 13129411]
19. Matveeva EG, Terpetschnig EA, Stevens M, Patsenker L, Kolosova OS, Gryczynski Z, Gryczynski I. Near-infrared squaraine dyes for fluorescence enhanced surface assay. Dyes Pigm. 2009; 80(1): 41–46. [PubMed: 20046935]
20. Almutairi A, Guillaudeu SJ, Berezin MY, Achilefu S, Frechet JM. Biodegradable pH-sensing dendritic nanoprobes for near-infrared fluorescence lifetime and intensity imaging. J. Am. Chem. Soc. 2008; 130(2):444–445. [PubMed: 18088125]
21. Kang J, Kaczmarek O, Liebscher J, Dahne L. Prevention of H-Aggregates Formation in Cy5 Labeled Macromolecules. Int J Polym Sci. 2010 ID 264781.

22. Pauli J, Licha K, Berkemeyer J, Grabolle M, Spieles M, Wegner N, Welker P, Resch-Genger U. New Fluorescent Labels with Tunable Hydrophilicity for the Rational Design of Bright Optical Probes for Molecular Imaging. Bioconjug. Chem. 2013

23. Pope, M.; Swenberg, CE. Electronic processes in organic crystals and polymers. New York: Oxford University Press; 1999. p. xxix-1328.

24. Kasha M, Rawls H, El-Bayoumi MA. The exciton model in molecular spectroscopy. Pure Appl. Chem. 1965; 11(3–4):371–392.

25. Rosch U, Yao S, Wortmann R, Wurthner F. Fluorescent H-aggregates of merocyanine dyes. Angew. Chem. Int. Ed. Engl. 2006; 45(42):7026–7030. [PubMed: 17013950]

26. Clegg, RM.; Sener, M. From Förster resonance energy transfer to coherent resonance energy transfer and back. International Society for Optics and Photonics; 2010. p. 75610C-75621C.

27. Yan Y, Marriott G. Analysis of protein interactions using fluorescence technologies. Curr.Opin. Chem. Biol. 2003; 7(5):635–640. [PubMed: 14580569]

28. Koushik SV, Vogel SS. Energy migration alters the fluorescence lifetime of Cerulean: implications for fluorescence lifetime imaging Forster resonance energy transfer measurements. J. Biomed. Opt. 2008; 13(3):031204. [PubMed: 18601528]

29. Ghukasyan V, Hsu CC, Liu CR, Kao FJ, Cheng TH. Fluorescence lifetime dynamics of enhanced green fluorescent protein in protein aggregates with expanded polyglutamine. J. Biomed. Opt. 2010; 15(1):016008. [PubMed: 20210454]

30. Dale RE, Eisinger J, Blumberg WE. The orientational freedom of molecular probes. The orientation factor in intramolecular energy transfer. Biophys. J. 1979; 26(2):161–193. [PubMed: 262414]

31. Censullo R, Martin J, Cheung H. The use of the isotropic orientation factor in fluorescence resonance energy transfer (FRET) studies of the actin filament. J. Fluoresc. 1992; 2(3):141–155. [PubMed: 24241625]

32. Benson RC, Kues HA. Fluorescence properties of indocyanine green as related to angiography. Phys. Med. Biol. 1978; 23(1):159–163. [PubMed: 635011]

33. Wurth C, Grabolle M, Pauli J, Spieles M, Resch-Genger U. Relative and absolute determination of fluorescence quantum yields of transparent samples. Nat. Protoc. 2013; 8(8):1535–1550. [PubMed: 23868072]

34. Wurth C, Pauli J, Lochmann C, Spieles M, Resch-Genger U. Integrating sphere setup for the traceable measurement of absolute photoluminescence quantum yields in the near infrared. Anal. Methods. 2012; 84(3):1345–1352.

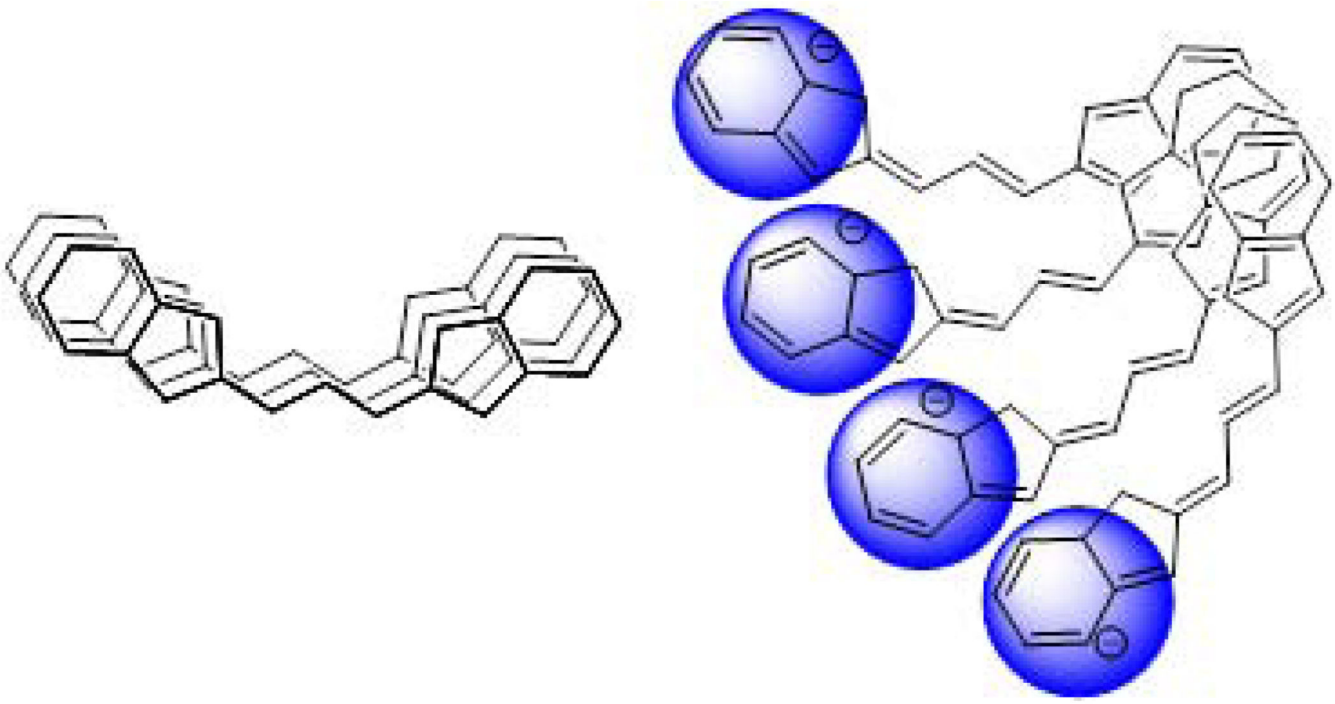

Figure 1.
Principle of the NIR dye (schematics) for minimum self-aggregation upon conjugation to proteins. Stacking causes dye self-aggregation, charged ends prevent dye from aggregating.

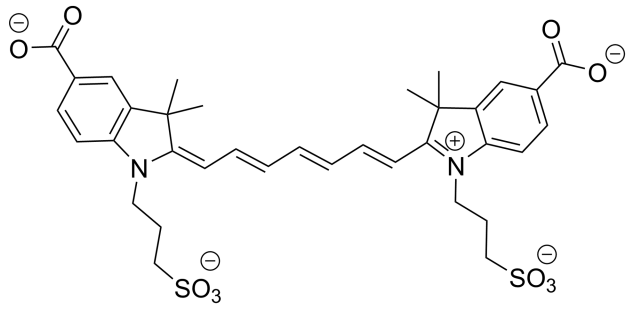

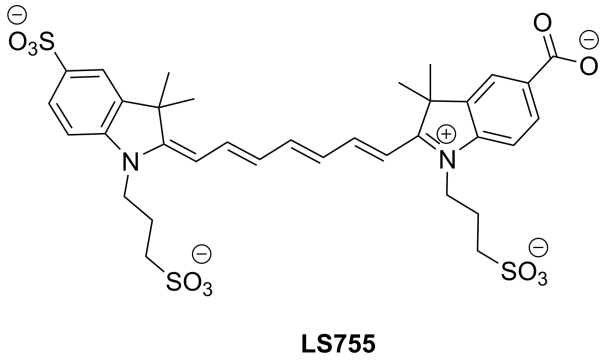

Figure 2.
Structures of LS601 and LS755

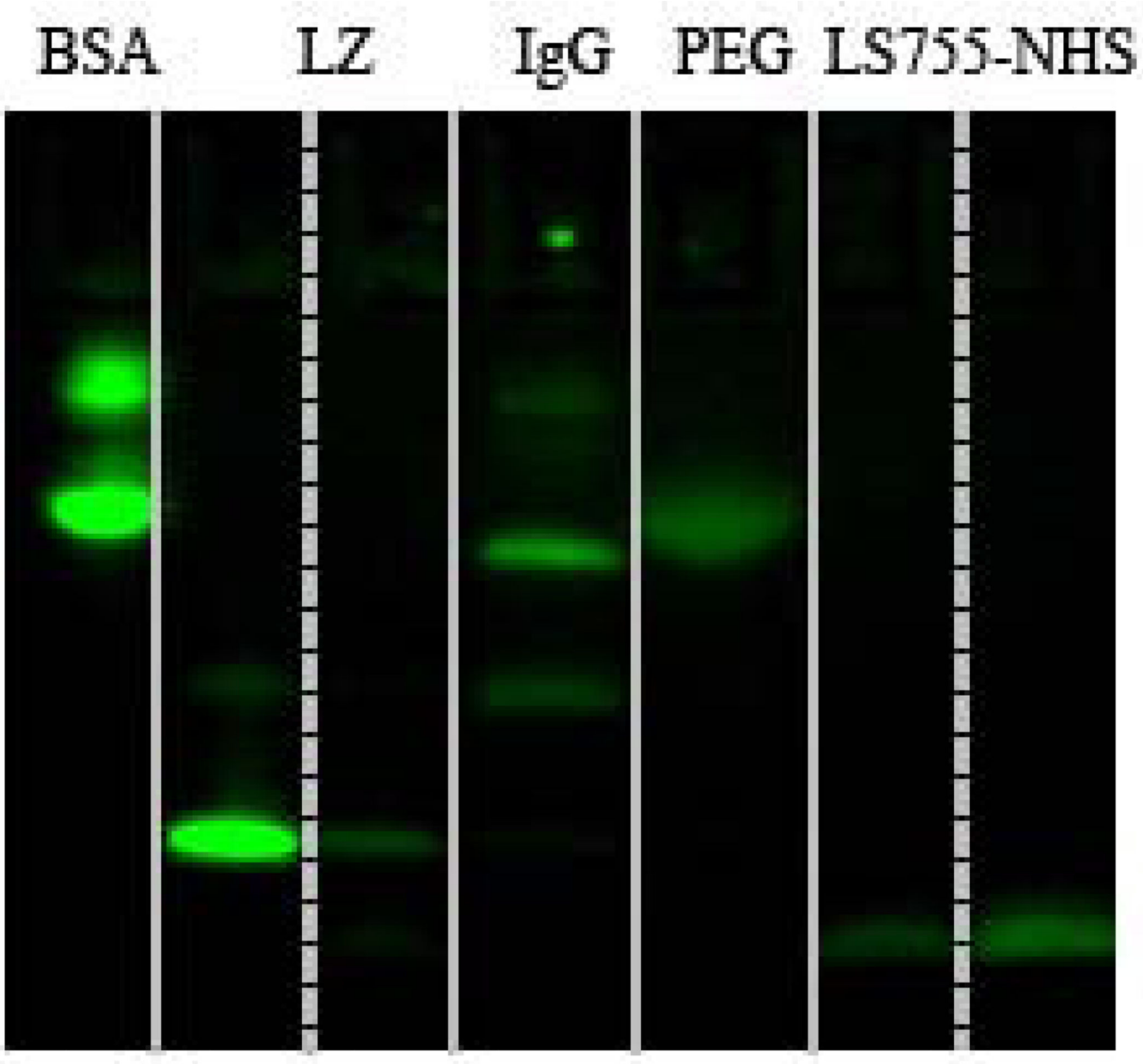

Figure 3.
SDS-PAGE of LS755-conjugates; ex/em: 735/800 nm. From left to right: LS755-BSA, LS755-Lz (two lanes of different well loading), LS755-IgG, LS755-PEG, LS755-NHS (two lanes of different well loading).

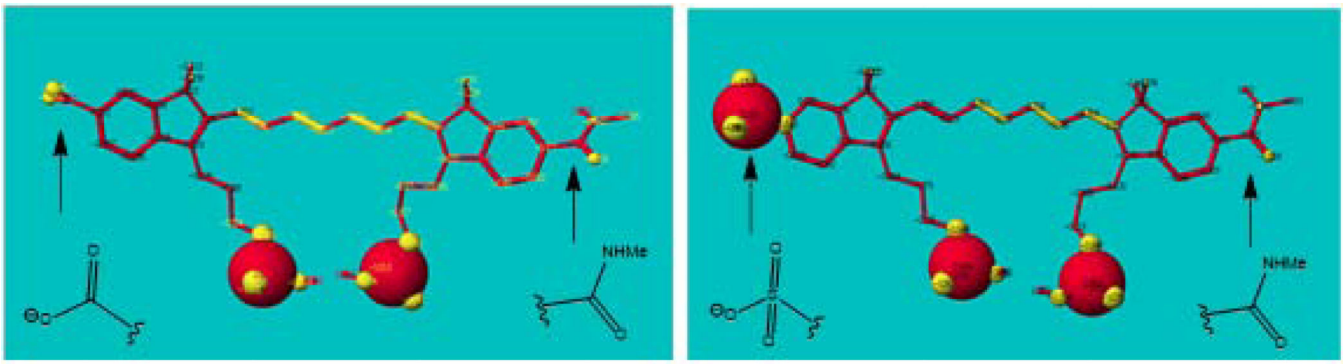

Figure 4.

Charge distribution of LS601 (left) and LS755 (right) pseudoconjugates. The charges are given using a sphere 0.5Å. Calculated using MM3/AM1 parameters implemented in Cache 5.0 modeling package.

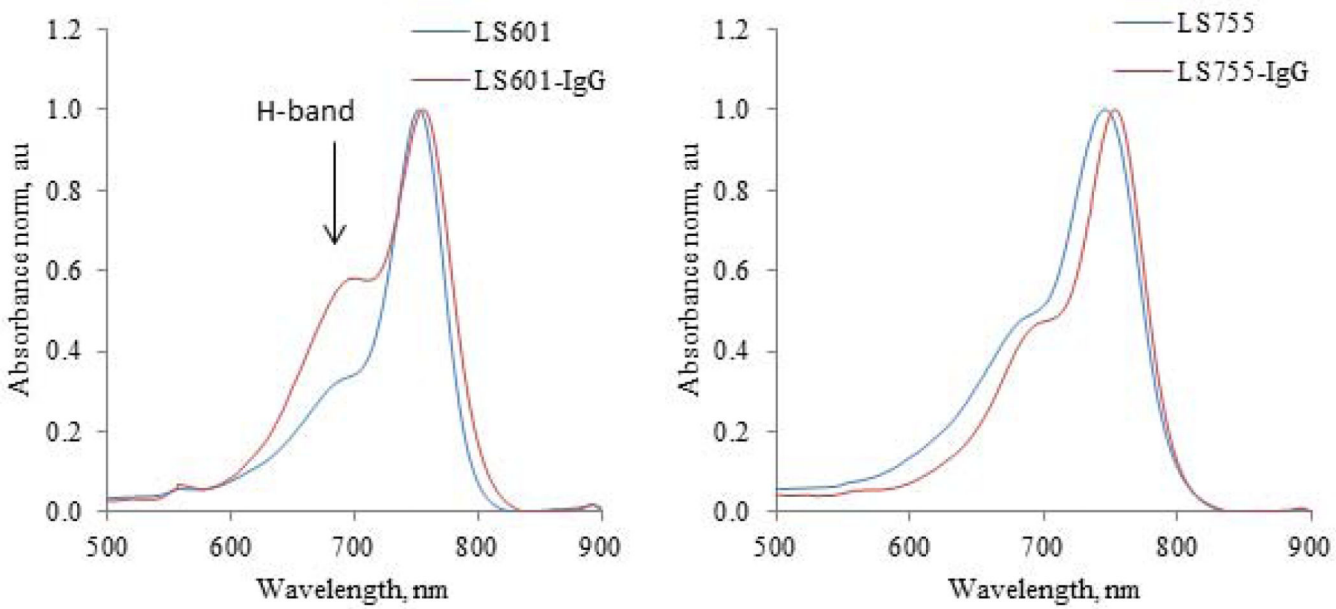

Figure 5.

Absorption spectra of IgG antibody labeled with LS601 and LS755. LS601 shows the presence of H-band that almost negligible in LS755-conjugates.

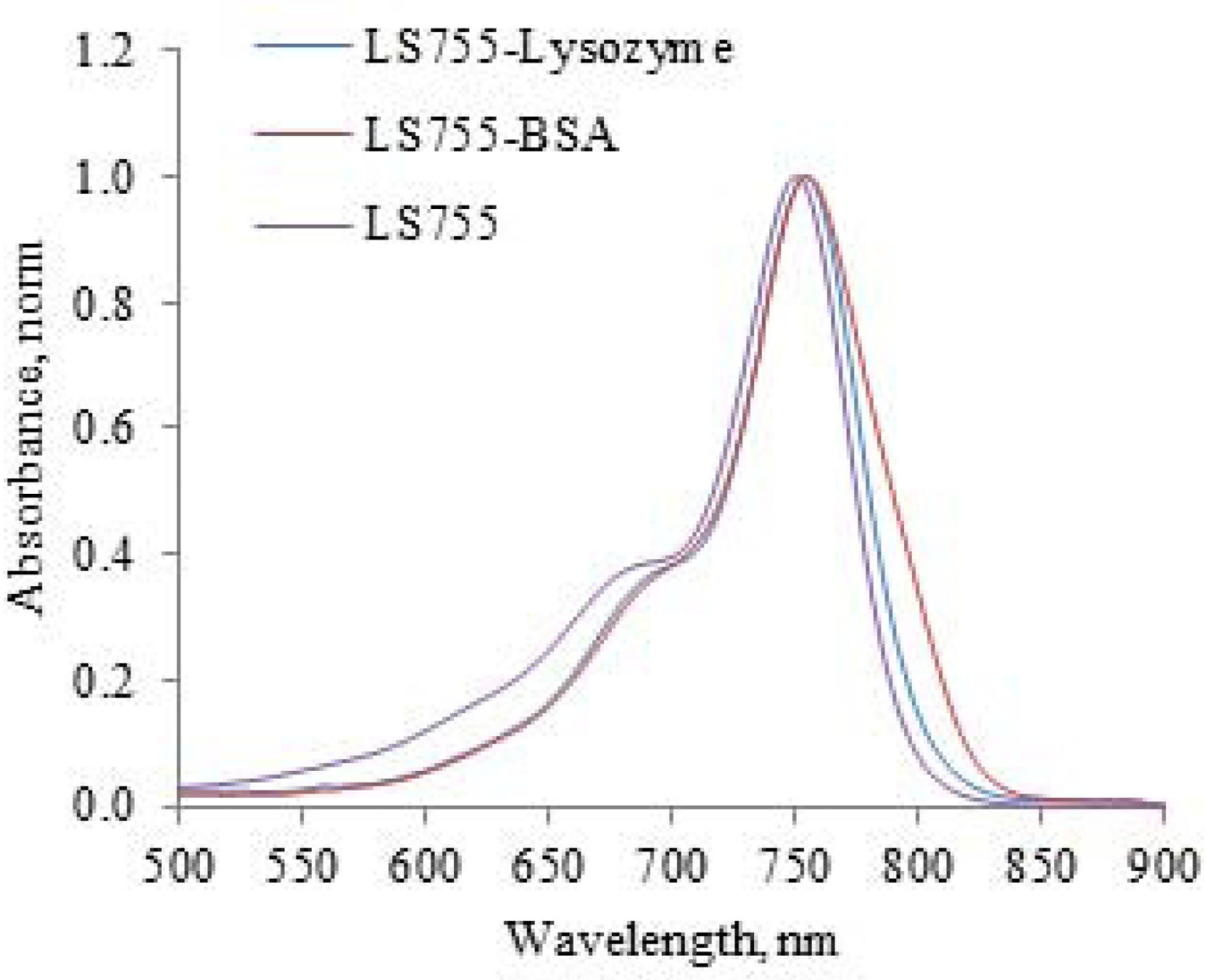

Figure 6.
Absorption of LS755-Lysozyme and LS-BSA conjugates show no presence of H-bands.

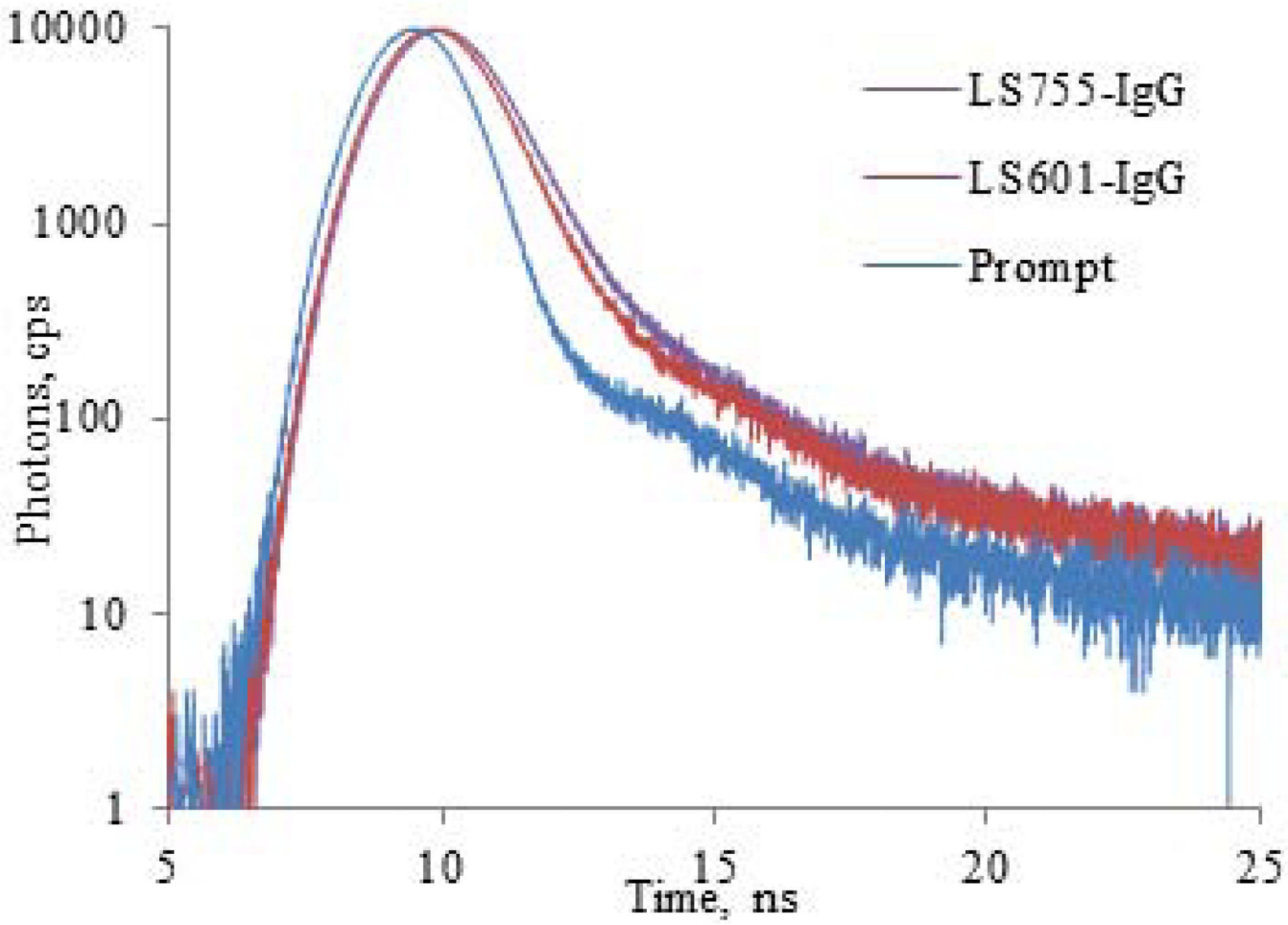

Figure 7.
Fluorescence decays of LS601-IgG and LS755-IgG conjugates (Ex/em. 740/790 nm).

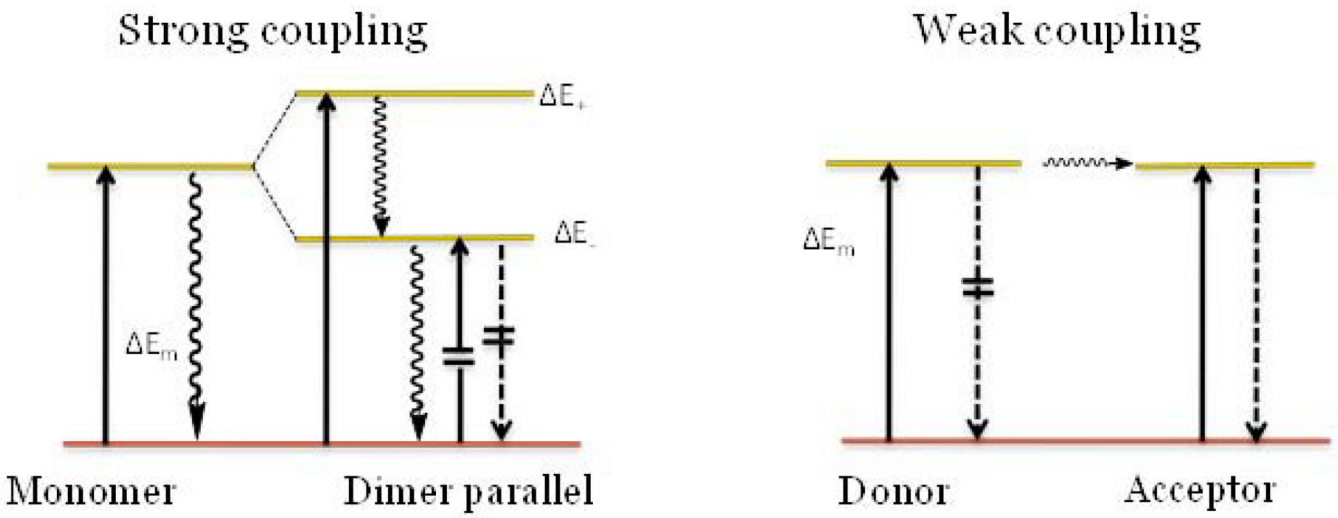

Figure 8.

Two mechanisms of quenching for molecules oriented parallel to each other. Left: strong coupling (Davydov splitting) leads to a blue shift in absorption and quenched fluorescence. Right: weak coupling (homoFRET) leads to no change in absorption but a change in emission. Solid arrows mark the absorption, dashed arrows the fluorescence, and wavy arrows the internal conversion; crossed lines are forbidden transitions.

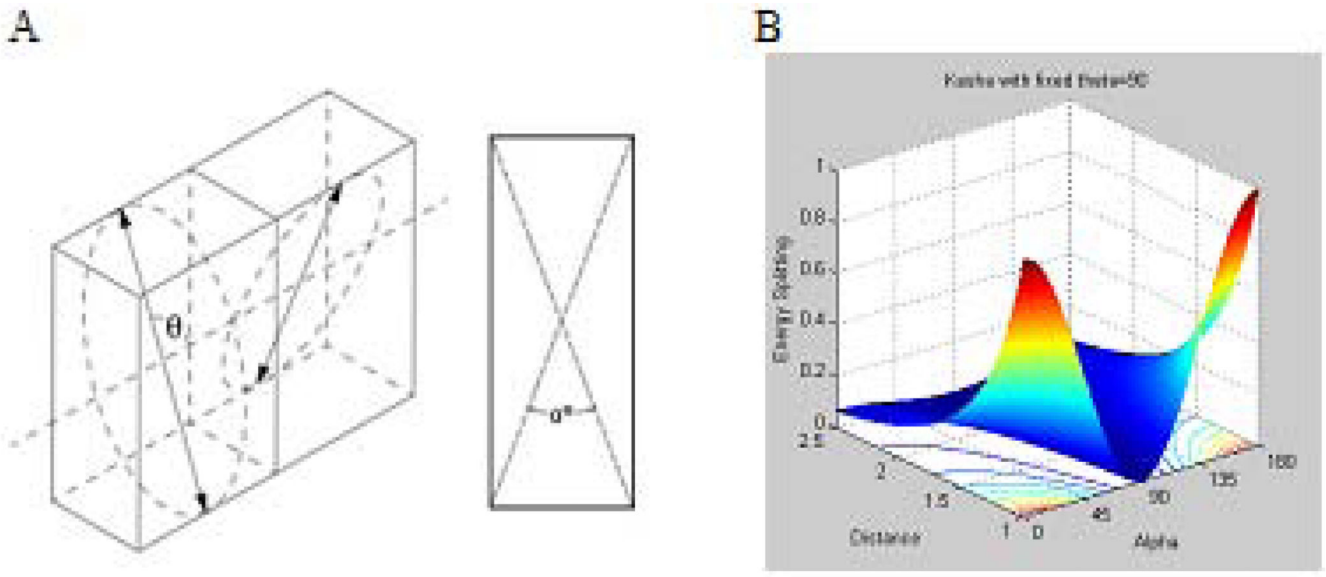

Figure 9.

Strong coupling. *A*: Spatial relationship between the two planes of interacting dye molecules, α represents an angle between the planes, and θ is the angle between the polarization axes and the line of molecular centers; *B*: modeling of the energy transfer as a function of *r* and α, with θ= 90° based on Eq. 1.

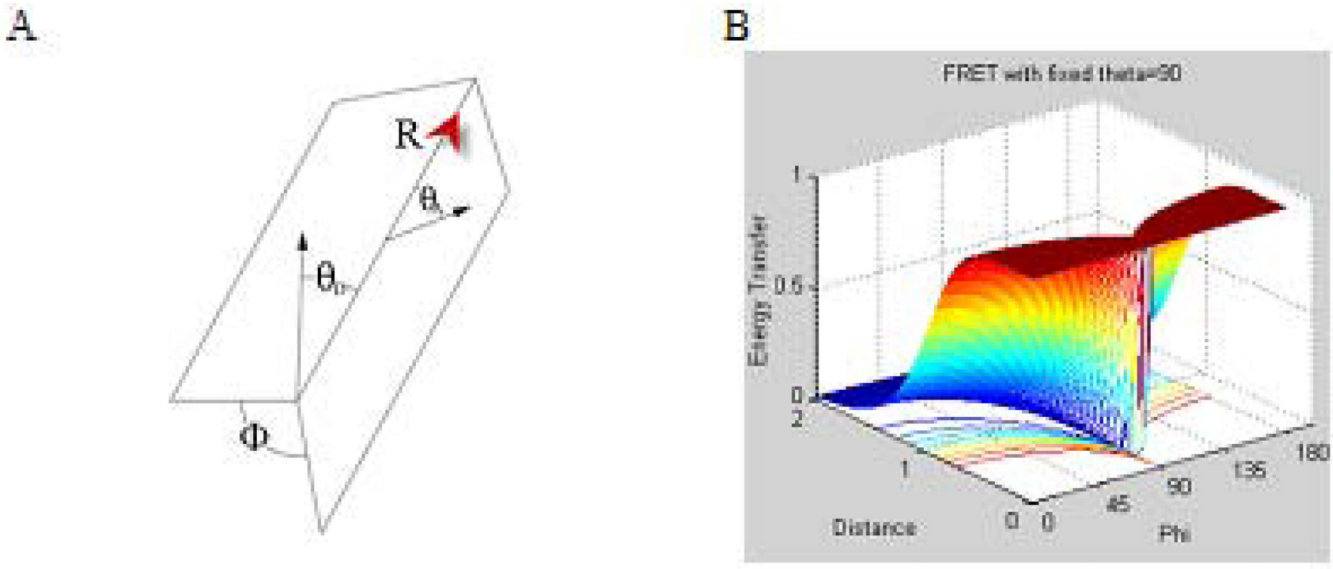

Figure 10.

Weak coupling *A*: Spatial relationship between the donor and acceptor dipoles. φ represents the angle between the planes defined separately by the donor and acceptor each with the vector R from the donor to the acceptor, θ_D is the angle between the donor dipole and R, θ_A is the angle between the acceptor dipole and R. *B*: The energy transfer profiles model based on eq. 2–3. Energy transfer as a function of distance and angle between the planes α with $\theta_D=\theta_A= 90°$ is the angle between the polarizations axes and the line of molecular centers.

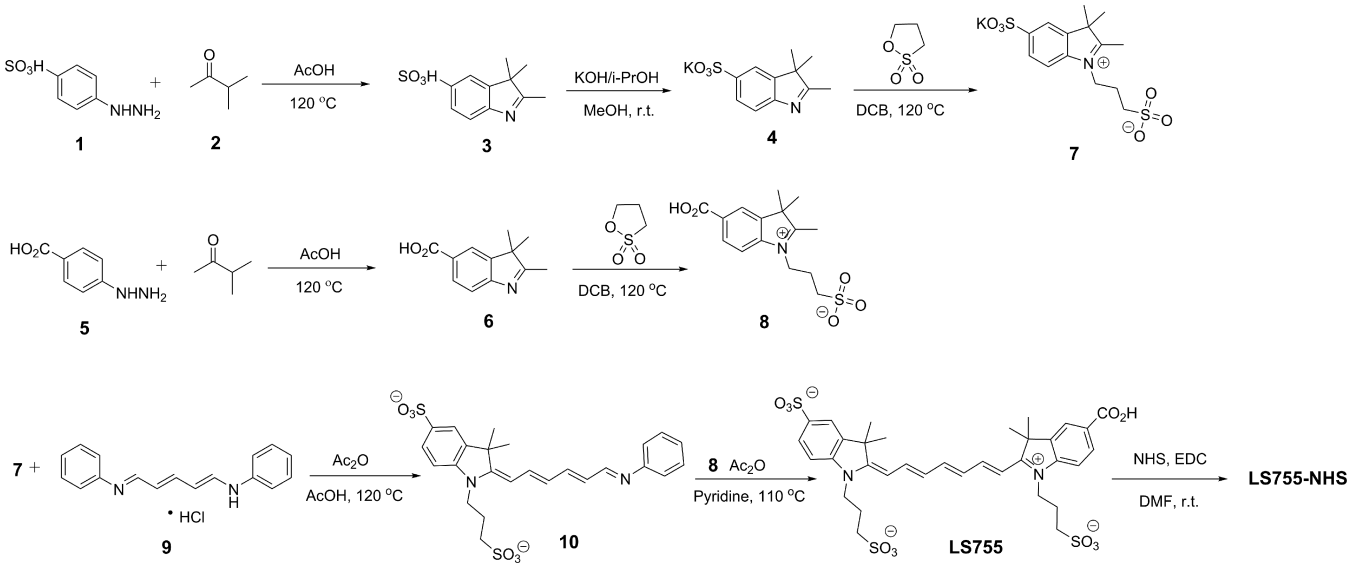

Scheme 1.
Synthesis of LS755 dye

Table 1

Optical probes of LS755 and dye-conjugates

Probe	MW, kDa	λ_{abs} (nm)	λ_{fl} (nm)	τ (ns)	Φ_{fl}	*r*
LS755	0.7	758[a]/745[c]	790[a]	1.21[a]/0.43[c]	0.260[a]/0.077[c]	0.155 +/−0.001[c]
LS755-IgG	150	755[c]	773[c]	0.65[b]	0.097[c]	0.239 +/−0.002[c]
LS755-BSA	67	755[c]	764[c]	0.96[b]	0.131[c]	0.201 +/−0.001[c]
LS755-Lz	15	754[c]	770[c]	0.73[b]	0.131[c]	0.222 +/−0.002[c]
LS601(8)	0.7	769[a]/752[c]	800[a]	1.29[a] /0.42[c]	0.200[a]	0.244 +/−0.002[c]
LS601-IgG(8)	150	757[c]	773[c]	0.53[c]	0.078[c]	0.311+/−0.008

a) DMSO,

b) 20% serum in water

c) water. MW – approximate molecular weight of the conjugate, λ_{abs} – absorption maximum, λ_{em} – emission maximum, Φ_{fl} - relative fluorescence quantum yield using a reference ICG in DMSO= 0.12 (32) (for using another value = 0.22 (33,34), the quantum yield has to be adjusted accordingly), *r* – fluorescence anisotropy.